Surface and Internal Excess Electron States in Molecular Clusters

R. N. Barnett and Uzi Landman

School of Physics, Georgia Institute of Technology, Atlanta, Georgia 30332

Dafna Scharf

IBM Research Laboratory, 8803 Rüschlikon, Switzerland

Joshua Jortner*

School of Chemistry, Sackler Faculty of Exact Sciences, Tel Aviv University, 69978 Tel Aviv, Israel

Excess Electrons in Clusters: An Overview

Clusters, i.e., finite aggregates containing $2-10^4$ atomic or molecular constituents, exhibit unique physical and chemical phenomena,[1-3] which provide ways and means to explore the gradual transition from molecular to condensed-matter systems. Furthermore, the large surface-to-volume ratio in clusters allows for the exploration of microscopic surface phenomena. The progress in our understanding of the evaluation of quantum, thermodynamic, dynamic, and chemical size effects in clusters is expected to provide a unified interrelationship between molecular, surface, and bulk phenomena in large finite systems.

We shall be concerned with the structural and dynamic implications of electron attachment to nonmetallic molecular clusters.[4-10] A classification of these systems, according to the strength of the intermolecular

binding in the cluster, the electron–cluster interactions, and the nature of the excess electron state, is provided in Table I. The theoretical methods currently available for the exploration of excess electron states in molecular clusters involve descriptive condensed-matter approximations,[11,12] quantum chemistry type self-consistent-field configuration interaction calculations,[13,14] the quantum path integral molecular dynamics (QUPID) approach,[15-24] and the adiabatic simulation method.[24,25] We have recently utilized[15-23] the QUPID method to explore the compositional, structural, and size dependence of electron localization in ionic and hydrogen-

Robert N. Barnett was born in Littlefield, TX, in 1947. He received a B.Sc. degree from Texas Tech University in 1976 and a Ph.D. degree in Physics from the University of Kansas in 1980. Between 1967 and 1971 he served in the U.S. Army. In 1980 he joined the School of Physics at the Georgia Institute of Technology, where he is currently a research scientist. His primary research interests are in condensed-matter, surface and materials science with a focus on the development of computer simulation methods.

Uzi Landman was born in Israel in 1944. He received his B.Sc. degree in Chemistry from the Hebrew University, an M.Sc. from the Weizmann Institute of Science, and a D.Sc. from the Technion, the Israel Institute of Technology, in 1969. Subsequently, he was at the Department of Chemistry, University of California, Santa Barbara, the Departments of Physics at the University of Illinois at Urbana–Champaign and the University of Rochester, and also the Webster Xerox Research Center. In 1977 he joined the School of Physics at the Georgia Institute of Technology in Atlanta, where he is a Regents Professor and Associate Dean for Research. In addition, he holds a Visiting Professorship in the School of Chemistry at Tel Aviv University, and between 1984 and 1987 he served as a Nordita Visiting Professor. His main research interests are condensed-matter and molecular dynamics phenomena, statistical mechanics, and surface science, with an emphasis on the development and application of classical and quantum simulations.

Dafna Scharf was born in Israel. She received her B.Sc. and M.Sc. degrees in chemistry from Tel Aviv University and her Ph.D. degree from Tel Aviv University in 1989. She is currently serving as a research assistant at IBM Research Laboratory, Rüschlikon, Switzerland. Her research interests are in the development and application of classical and quantum simulations of clusters and condensed phases.

Joshua Jortner was born in Poland in 1933. He received his M.Sc. degree in Chemistry and Physics for the Hebrew University and his Ph.D. degree in Physical Chemistry from the Hebrew University in 1960. He served as a faculty member at the Hebrew University and the University of Chicago. In 1965 he joined Tel Aviv University, where he is presently serving as the Heinemann Professor of Chemistry. His main research interests are in the area of chemical physics, focusing on dynamic processes in molecules, clusters, and condensed phases.

(1) Jortner, J. *Ber. Bunsen-Ges. Phys. Chem.* **1984,** *88,* 188.
(2) *Elemental and Molecular Clusters*; Benedek, G., Martin, T. P., Pacchioni, G., Eds.; Springer Verlag: Berlin, 1988.
(3) *Large Finite Systems*; Jortner, J., Pullman, A., Pullman, B., Eds.; B. Reidel: Dordrecht, 1987.
(4) Haberland, H.; Langosch, H.; Schindler, H. G.; Worsnop, D. R. *Surf. Sci.* **1985,** *156,* 157.
(5) Haberland, H.; Schindler, H. G.; Worsnop, D. R. *J. Chem. Phys.* **1984,** *81,* 3742.
(6) Haberland, H.; Schindler, H. G.; Worsnop, D. R. *Ber. Bunsen-Ges. Phys. Chem.* **1984,** *88,* 270.
(7) Knapp, M.; Echt, O.; Kreisle, D.; Recknagel, E. *J. Chem. Phys.* **1986,** *85,* 636.
(8) Knapp, M.; Echt, O.; Kreisle, D.; Recknagel, E. *J. Phys. Chem.* **1987,** *91,* 2601.
(9) Bowen, K. H. *Z. Phys. D,* in press.
(10) Haberland, H.; Richter, T. *Z. Phys. D.* **1988,** *10,* 99.
(11) Springer, B. E.; Jortner, J.; Cohen, M. H. *J. Chem. Phys.* **1968,** *48,* 2720.
(12) Stampfli, P.; Bennemann, K. H. *Phys. Rev. Lett.* **1978,** *58,* 2635.
(13) Newton, M. *J. Chem. Phys.* **1973,** *58,* 5833.
(14) Rao, B. K.; Kestner, N. R. *J. Chem. Phys.* **1984,** *80,* 1587.
(15) For a recent review, see: Berne, B. J.; Thirumalai, D. *Annu. Rev. Phys. Chem.* **1986,** *37,* 401.
(16) Landman, U.; Scharf, D.; Jortner, J. *Phys. Rev. Lett.* **1985,** *54,* 1860.
(17) Scharf, D.; Jortner, J.; Landman, U. *Chem. Phys. Lett.* **1986,** *126,* 495.
(18) Scharf, D.; Jortner, J.; Landman, U. *J. Chem. Phys.* **1988,** *88,* 4273.
(19) Landman, U.; Barnett, R. N.; Cleveland, C. L.; Scharf, D.; Jortner, J. *J. Phys. Chem.* **1987,** *91,* 4890.
(20) Barnett, R. N.; Landman, U.; Cleveland, C. L.; Jortner, J. *Phys. Rev. Lett.* **1987,** *59,* 811.
(21) Barnett, R. N.; Landman, U.; Cleveland, C. L.; Jortner, J. *J. Chem. Phys.* **1988,** *88,* 4421, 4429.
(22) Barnett, R. N.; Landman, U.; Jortner, J. *Chem. Phys. Lett.* **1988,** *145,* 382.
(23) Barnett, R. N.; Landman, U.; Kestner, N. R.; Jortner, J. *J. Chem. Phys.* **1988,** *88,* 6670.
(24) Rossky, P. J.; Schnitker, J. *J. Phys. Chem.* **1988,** *92,* 4277.
(25) Barnett, R. N.; Landman, U.; Nitzan, A. *J. Chem. Phys.* **1988,** *89,* 2242.

Table I
Electron Attachment to Clusters

type of cluster	nature of excess electron state	canonical example	cause of electron binding
rare gas $(He)_n$	surface state localized	$(He)_n^-$	repulsive + weak polarization
heavy rare gas	bulk state extended	$(Xe)_n^-$	dominated by attractive interactions
van der Waals	stable negative molecular ion	$(SF_6)_n^-$	large electron affinity of a single molecule
van der Waals	solvated negative ion	$(CO_2)_n^-$	positive electron affinity of a single molecule; stabilization of a negative ion by solvation
H-bonded	diffuse localized state	$(H_2O)_2^-$	weak charge dipole
H-bonded	surface state localized interior (bulk) state, localized (large n)	$(H_2O)_n^-$ $(11 \le n < 64)$ $(NH_3)_n^-$ $(n \ge 35)$ $(H_2O)_n^-$ $(n \ge 64)$	electron–polar molecule attraction in conjunction with large cluster reorganization
ionic	electron localization in anion vacancies; surface states	$(Na_nCl_m)^{m-n+1}$	electrostatic interactions

bonded clusters, which provide novel information regarding three central phenomena. Firstly, the electron localization modes in large finite systems are elucidated, resulting in novel phenomena of the formation of energetically stable surface states and interior states of an excess electron in clusters. Secondly, electron attachment provides a novel mechanism for the induction of configurational rearrangement of clusters, which is investigated in the general context of the interesting problem of isomerization and melting of clusters.[26,27] Thirdly, quantitative information regarding structural and energetic size effects emerged, which provides a central contribution to the merging between microscopic and macroscopic points of view in the description of the "transition" from finite large systems to bulk fluids.

Theoretical Arsenal: The Quantum Path Integral Molecular Dynamics Method

The QUPID method,[15-24] which rests on a discrete version of Feynman's path-integral method,[28] provides a powerful approach to explore the structure and energetics of excess electron states in clusters. Consider an electron interacting with a cluster of N particles via a potential V_e which is specified by the Hamiltonian

$$H = -\frac{\hbar^2}{2m}\nabla^2 + V_e(r) \tag{1}$$

The partition function for such a system is

$$Z = \text{Tr}\,[\exp(-\beta H)] \tag{2}$$

where $\beta = 1/k_B T$ is the inverse temperature, and the energy of the system is given by

$$E = -\frac{\partial}{\partial \beta}\ln Z \tag{3}$$

An isomorphism between the quantum problem and an appropriate classical problem is established by (a) the factorization of the partition function into P contributions and by (b) invoking a small β/P expansion for the matrix elements. This procedure allows for the expression of the partition function

$$Z \simeq \left(\frac{Pm}{2\pi\hbar^2\beta}\right)^{3P/2}\int d\vec{r}_1...d\vec{r}_P \exp[-\beta V_{\text{eff}}(\vec{r}_1...\vec{r}_P)] \tag{4}$$

in terms of the effective potential

$$V_{\text{eff}} = \sum_{i=1}^{P}\left[\frac{Pm}{2\hbar^2\beta^2}(\vec{r}_1 - \vec{r}_{i+1})^2 + \frac{1}{P}V_e(\vec{r}_i)\right] \tag{5}$$

which consists of a superposition of a harmonic potential and the cluster potential.

Equations 4 and 5 establish an (approximate) isomorphism[15] between the quantum problem characterized by the Hamiltonian H, eq 1, and the classical problem defined by the effective potential, eq 5. In the isomorphic classical problem, the electron is mapped onto a closed chain (necklace) of P pseudoclassical particles (bead). Each point of the necklace exerts two types of interactions, (1) nearest-neighbor interactions between the beads in the chain, which are characterized by a harmonic potential with a force constant $Pm/\hbar^2\beta^2$, and (2) interactions with the cluster through the scaled potential $V_e(\vec{r})/P$. The average energy of the system is

$$E = \frac{3N}{2\beta} + \langle V \rangle + E_e \tag{6}$$

$$E_e = K_e + \frac{1}{P}\langle\sum_{i=1}^{P}V_e(\vec{r}_i)\rangle \tag{7}$$

The first two terms in eq 6 correspond to the kinetic energy, $3N/2\beta$, and the potential energy, $\langle V \rangle$, of the classical N-particle cluster. E_e, eq 7, is the electron energy, which contains kinetic and potential contributions. The electron kinetic energy is[29]

$$K_e = \frac{3}{2\beta} + \frac{1}{2P}\sum_{i=1}^{P}\left\langle\frac{\partial V_e(\vec{r}_i)}{\partial\vec{r}_i}\cdot(\vec{r}_i - \vec{r}_P)\right\rangle \tag{8}$$

consisting of a free-particle term, $3/2\beta$, and the contribution K_{int} from the interaction with the ions. The indicated statistical averages $\langle\,\rangle$ are over the Boltzmann distribution as defined in eq 4. This formalism is converted into a numerical algorithm by noting the equivalence of the sampling described above to that over phase space trajectories generated via molecular dynamics by the classical Hamiltonian.

The energetics of an excess electron cluster is expressed in terms of the electron vertical binding energy EVBE = E_e and the electron adiabatic binding energy

$$\text{EABE} = \text{EVBE} + E_c \tag{9}$$

where the cluster reorganization energy is $E_c = \langle V \rangle -$

(26) Berry, R. S.; Beck, T. L.; Davis, H. L.; Jellinek, J. *Adv. Chem. Phys.* 1988, 70, 74.
(27) Jortner, J.; Scharf, D.; Landman, U., ref 2, p 148.
(28) Feynman, R. P.; Hibbs, A. R. *Quantum Mechanics and Path Integrals*; McGraw-Hill: New York, 1965.

(29) Herman, M. F.; Bruskin, E. J.; Berne, B. J. *J. Chem. Phys.* 1983, 79, 5063.

352 *Acc. Chem. Res., Vol. 22, No. 10, 1989*

Barnett et al.

98.88

$Na_{14}Cl_{13}^{+}$

91.35

$Na_{14}Cl_{12}^{++}$

Figure 1. Configurations of some small and large charged NaCl clusters to which an excess electron was attached.[31] The numbers refer to the ground-state energies in eV units.

$\langle V \rangle_0$, being the difference between the equilibrium intermolecular and intramolecular potential energies in the cluster containing an excess electron cluster and in the neutral cluster, respectively. $-EVBE$ is the detachment energy of the electron from the cluster without allowing for nuclear rearrangement, which is measured by photoelectron spectroscopy. EABE is the heat of solution of the excess electron in the cluster, with EABE < 0 corresponding to an energetically stable bound state.

The charge distribution is characterized by the radius of gyration, R_g, of the excess electron. The degree of localization can be assessed by comparing R_g to the thermal wavelength $\lambda_T = (\beta \hbar^2/m)^{1/2}$ of the electron.

Electron Localization in F Centers and Surface States in Alkali Halide Clusters

The compositional, structural, and size dependence of various electron localization modes in ionic alkali halide clusters (AHCs) have been explored by using QUPID simulations.[16] The AHC is treated as a classical system. The interionic potential within the AHC is given by the Born–Mayer recipe.[30] The e–AHC potential consists of a sum of electron–ion potentials. These are described by a purely repulsive pseudopotential $\phi_{eX^-}(r) = e^2/r$ for electron–anion interaction, while the electron–cation interactions are given by the local truncated Coulomb pseudopotential $\phi_{eM^+}(r) = -e^2/R_c$ for $r \leq R_c$ and $\phi_{eM^+}(r) = -e^2/r$ for $r > R_c$. The electron–cation pseudopotential parameters were varied by changing the cutoff radius R_c with a typical value chosen for Na$^+$ being $R_c = 3.22a_0$.

Structural[31] and classical molecular dynamics[27] calculations have established that, when the size of the ionic cluster increases ($N \geq 20$), NaCl crystallographic arrangement is energetically preferred even if the number of positive and negative ions is not equal. We studied the interaction of an electron with the positive clusters $[Na_{14}Cl_{13}]^+$ and $[Na_{14}Cl_{12}]^{2+}$, which exhibit the crystallographic structure without and with a vacancy, respectively (Figure 1), and which are characterized by a pronounced energetic stability.[31] In Figure 2, we present our results for the equilibrium charge distribution of the electron necklace edge points and for the nuclear configuration of the clusters.

As is apparent from Figure 2a, the $[Na_{14}Cl_{12}]^{2+}$ cluster stabilizes an internally localized excess electron state. The features of the internal electron localization are as follows: (1) It occurs in a moderately large cluster. (2) An anion vacancy is required. (3) The localized electron state is surrounded by Na$^+$ ions in an octahedral configuration and by twelve Cl$^-$ ions. (4) The ionic con-
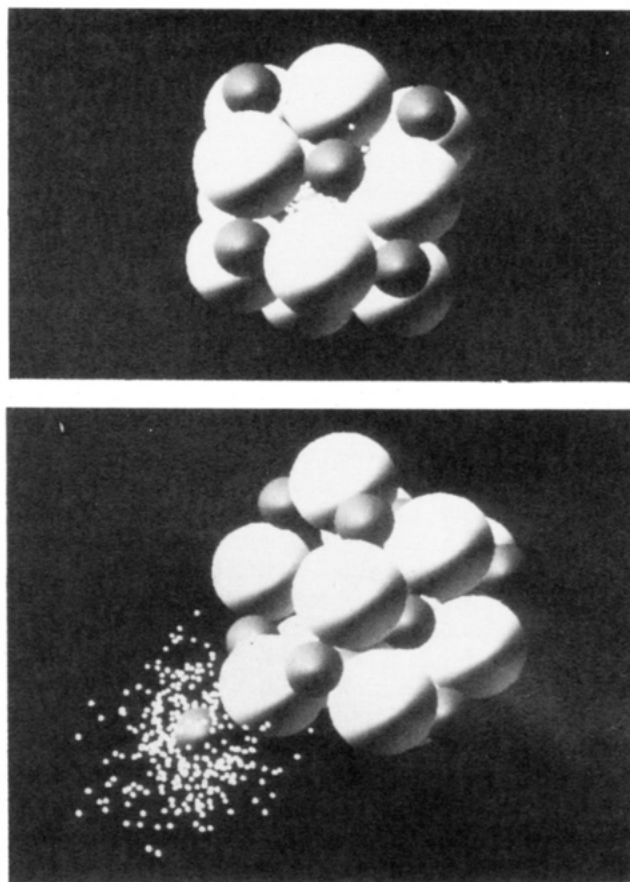
(30) Fumi, F. G.; Tosi, M. P. *J. Phys. Chem. Solids* **1964**, *31*, 45.
(31) Martin, T. P. *Phys. Rep.* **1983**, *95*, 169.

Figure 2. Ionic configuration and electron necklace distributions for excess electron interacting with large $[Na_nCl_m]^{n-m}$ clusters ($R_c = 3.22$ au). Small and large spheres correspond to Na$^+$ and Cl$^-$ ions, respectively.[16] Dots represent the "electron beads". (a) Top: e–$[Na_{14}Cl_{12}]^{2+}$. Internal localization is in an anion vacancy. EVBE = -6.77 eV, EABE = -4.6 eV, E_c = 2.17 eV. (b) Bottom: e–$[Na_{14}Cl_{13}]^+$. Surface localized state. EVBE = -4.34 eV, EABE = -1.47 eV, E_c = 2.87 eV. Reprinted with permission from ref 19. Copyright 1987 American Chemical Society.

figuration is somewhat distorted. (5) The gain in EVBE exceeds the loss in E_c, i.e., EABE < 0, which favors localization. (6) The total energy of e–$[Na_{14}Cl_{12}]^{2+}$ is close to that of the $[Na_{14}Cl_{13}]^+$, whereupon the electron (internal) binding energy in the cluster is similar to that of a negative ion. (7) These results establish the dominance of short-range attractive interactions for internal electron localization. (8) The spatial extent of the charge distribution is characterized by the radius of gyration whose components assume the values[16] $R_g = (5–10)a_0$. The thermal wavelength of a free electron at $T = 300$ K is $\lambda_T = 56a_0$. Accordingly, for the internal excess electron state, $R_g \ll \lambda_T$ demonstrates enhanced localization.

The internal excess electron state in the $[Na_{14}Cl_{12}]^{2+}$ cluster bears a close analogy to the F center in macroscopic alkali halide crystals[32] and in their melts.[33]

A drastically different localization mode is obtained in the $[Na_{14}Cl_{13}]^+$ system (Figure 2b), where a novel surface state is exhibited.[16] Such surface states were considered for alkali halide crystals by Tamm[32] about 50 years ago, but were never experimentally documented. The characteristics of external localization of

(32) Mott, N. F.; Gurney, R. W. *Electronic Processes in Ionic Crystals*; Oxford University: Oxford, 1946.
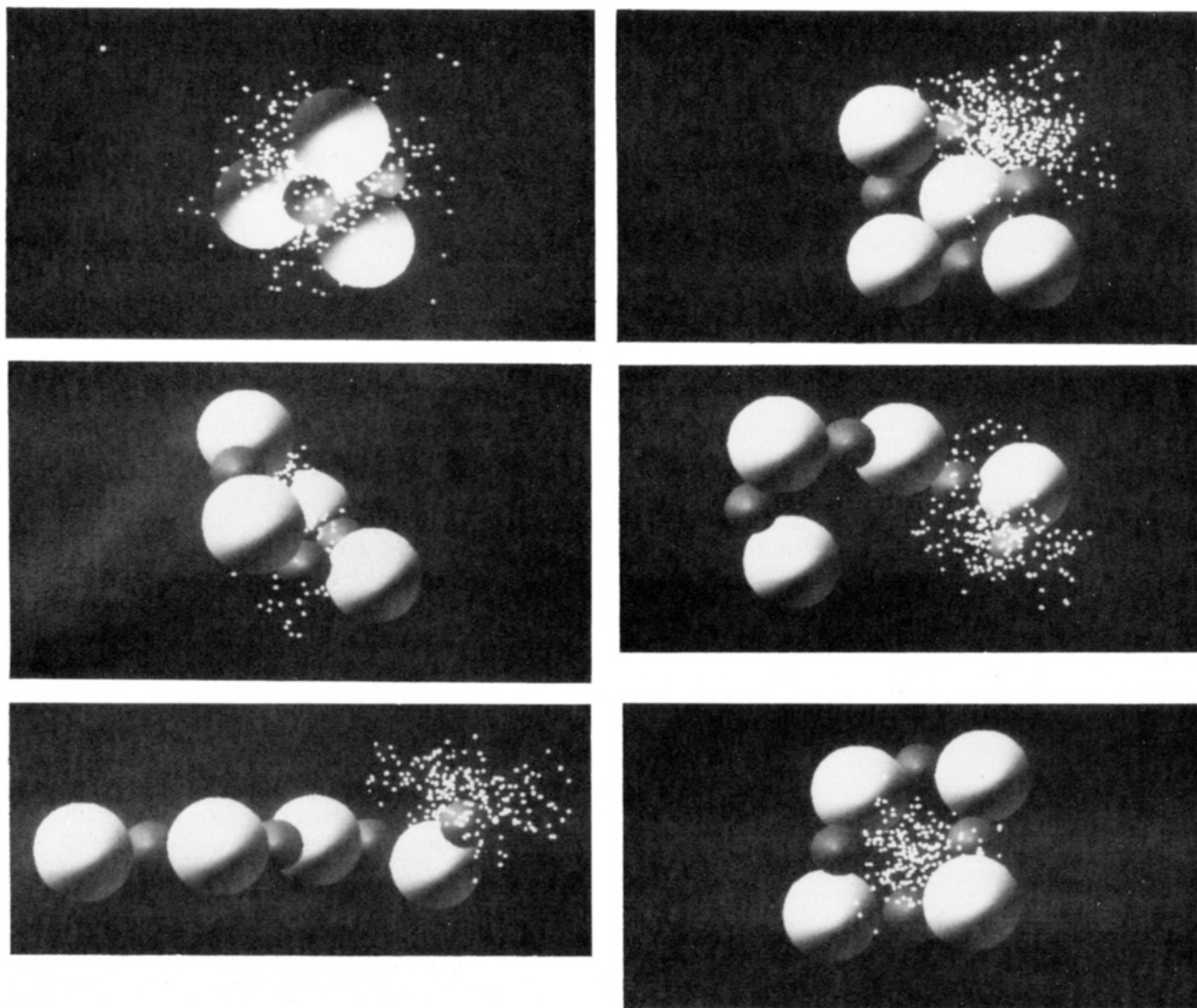(33) Pitzer, K. S. *J. Am. Chem. Soc.* **1962**, *84*, 2025.

Figure 3. Cluster configurations and "electron necklace" distribution for an excess electron with a Na_4Cl_4 cluster.[18] Left to right: top, (a) 50 K, (b) 575 K; middle, (c, d) 750 K; bottom, (e, f) 1000 K. Parts a–c, e, and f reprinted with permission from ref 19. Copyright 1987 American Chemical Society.

an electron on an NaCl cluster are as follows: (1) It is exhibited in a vacancy-free moderately large AHC. (2) In such an AHC, internal localization is prohibited by a large value of E_c. (3) The excess electron in $[Na_{14}Cl_{13}]^+$ localizes around Na^+ surface ions, leaving a neutral $Na_{13}Cl_{13}$ cluster interacting with a partially neutralized Na atom. (4) In this system a surface localized electron state is exhibited. (5) For clusters containing heavier M^+ ions, the surface state will become more extended. (6) The observation of the localization of an excess electron around a single surface Na^+ ion in the center of the face of $[Na_{14}Cl_{13}]^+$, rather than a delocalized surface state, manifests symmetry breaking effects induced by vibrational excitations at a finite temperature.

Cluster Isomerization Induced by Electron Attachment

Cluster structural rearrangement induced by the attachment of an excess electron is prevalent in small ionic clusters.[16] In view of the intimate interrelationship between structural isomerization and melting of clusters, it will be interesting to explore the isomerization of such finite systems induced by electron localization

in small neutral ionic clusters. Electron localization induces configurational transformations in small neutral ionic clusters at relatively low temperatures, and the equilibrium configurations of the cluster with the attached electron do not necessarily relate to those of the parent neutral cluster.[18] Our QUPID studies[18] of electron interaction with Na_4Cl_4 clusters at the temperature range 50–1000 K employed the interaction potentials previously described, modified to include electron–anion polarizability interaction. Equilibrium configurations at various temperatures are shown in Figure 3. At low temperature ($T \leq 500$ K), the electron distribution is extended with an equal probability charge distribution around all four Na^+ ions, and the ionic configuration is similar to that of the low-temperature neutral cluster. At the intermediate temperature domain, 500 K $\leq T \leq 750$ K, a configurational change of the negative cluster is exhibited (see Figure 3). This is a distorted planar configuration which is similar to the stable structure of the related classical $Na_4Cl_5^-$ cluster, and which we found in simulations performed in the temperature range 50 K $< T < 1100$ K. At the high-temperature domain, 750 K $< T < 1200$ K, a coexistence of several isomers is found. At $T \sim 750$ K, a boat-like configuration dominates (while a bent

chain is also encountered), and at $T \sim 1000$ K, an elongated chain is found in coexistence with a planar ring (Figure 3). We observe a tendency toward spatial localization of the electron upon increases in T. Furthermore, the presence of the excess electron induces two types of configurational modifications: (1) The localized excess electron can play the role of a negative ion, with appreciable kinetic energy, which is overwhelmed by the potential energy of the electron in the field of the ions. Consequently, new nuclear configurations of the negative cluster, which have no counterpart in the neutral cluster, will be exhibited. (2) The partial neutralization of a single positively charged ion by the excess electron results in the appearance of the high-temperature configurations of the neutral parent cluster at substantially lower temperatures for the negatively charged cluster.

Excess Electron in Water Clusters: Genesis

The existence of the solvated electron was experimentally demonstrated in 1863 for liquid ammonia[34] and in 1962 for water.[35] Electron localization in these and other polar fluids is nonreactive, involving cooperative solvation, which originates from the combination of long-range[36] and short-range[37] attractive interactions and is accompanied by a large local solvent reorganization.[37] During the last decade, the problem of the electron localization in a finite cluster of polar molecules[4-10] constituted a theoretical challenge for the elucidation of distinct surface and interior localization modes in finite systems and the delicate dependence of their stability on the nature of electron–molecule and intermolecular interactions. The following experimental information emerged regarding size effects on electron attachment to water and ammonia clusters:[4-9] (1) The water dimer constitutes the smallest water cluster which attaches an electron, resulting in a weakly bound $(H_2O)_2^-$ state, with a vertical binding energy of 34 meV obtained from photoelectron spectroscopy.[9] (2) Electron attachment to small $(H_2O)_n^-$ clusters for all n but $n = 4$ was documented. (3) Strongly bound $(H_2O)_n^-$ clusters are observed for $n \geq 11$. (4) Photoelectron spectroscopy[9] gave vertical electron binding energies for $(H_2O)_n^-$ with $n = 2, 5, 6$, and 11–40. (5) Nonreactive electron localization in water clusters was experimentally documented to originate either from electron binding during the cluster nucleation[4-6] process or by electron attachment to preexisting clusters.[7,8] (6) A striking difference is exhibited between the lowest coordination number for the formation of strongly bound $(H_2O)_n^-$ ($n \geq 11$) and of $(NH_3)_n^-$ ($n \geq 35$).[4-6]

The Dilemma

The experimental observation of strongly bound $(H_2O)_n^-$ ($n \geq 11$) clusters poses a challenging theoretical problem, as the origin of the energetic stability of these excess electron clusters is not clear. Quantum mechanical calculations for $(H_2O)_6^-$ and $(H_2O)_8^-$ [14] and QUPID calculations for $(H_2O)_{18}^-$ [19,20] with the electron in an interior state have established the occurrence of
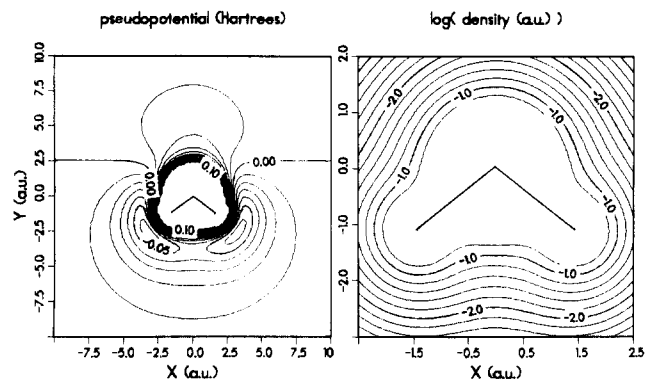

Figure 4. Contours of electron–water interactions, left, and of the electronic density of H_2O ($\log_{10} \rho(r)$), in the plane containing the nuclei. The oxygen is located at the origin.[20,21] Reprinted with permission from ref 19. Copyright 1987 American Chemical Society.

large cluster reorganization energies and positive adiabatic electron binding energies, precluding the existence of such interior excess electron clusters.[20,27] These conclusions are in contrast with experiment.[4-9] These theoretical studies followed faithfully the conventional wisdom in the field of solvated electron theory,[34,36,37] invoking the implict assumption that the excess electron state in $(H_2O)_n^-$ ($n = 6, 8, 18$) constitutes an interior localization mode. On the basis of QUPID simulations it was established that electron localization in small ($n = 2$)[19,38] and medium-sized[20-22] ($8 \leq n < 64$) water clusters does not involve an interior state, but rather constitutes a novel excess electron surface state on polar clusters.

Interactions in $(H_2O)_n^-$ and $(NH_3)_n^-$ Clusters

A key issue in modeling the system by QUPID simulations rests on the choice of interaction potentials. We have used a newly developed electron–molecule pseudopotential, which consists of Coulomb, polarization, exclusion, and exchange contributions,[20-23] $V = V_{coul} + V_p + V_e + V_x$ (Figure 4). The Coulomb interaction V_{coul} was represented by point charges, which were chosen to give a good representation of the dipole and quadrupole moments of H_2O. The polarization interaction V_p was chosen to fit the adiabatic polarization potential. The exclusion, V_e, and exchange, V_x, contributions both require the electron charge density ρ of the water molecule (Figure 4). The exclusion repulsive interaction was modeled as a "local kinetic energy", i.e., $V_e \propto \rho^{2/3}$. The exchange interaction was modeled by a local approximation $V_x \propto \rho^{1/3}$, with the proportionality parameter being fit to obtain agreement between a QUPID result and the SCF calculation[14] at a fixed nuclear configuration. A similar pseudopotential was constructed for e–NH_3 interactions.[23] Known intra- and intermolecular interactions for water[39] and ammonia[40] were employed.

Surface Excess Electron States on Medium-Sized Water Clusters

Our QUPID studies[20-22] of the energetics and struc-

(34) Weyl, W. *Ann. Phys. (Leipzig)* **1963**, *197*, 601.
(35) Hart, E. J.; Boag, J. W. *J. Am. Chem. Soc.* **1962**, *84*, 4090.
(36) Jortner, J. *J. Chem. Phys.* **1959**, *30*, 839.
(37) Copeland, D. A.; Kestner, N. R.; Jortner, J. *J. Chem. Phys.* **1970**, *53*, 1189.

(38) Wallquist, A.; Thirumalai, D.; Berne, B. J. *J. Chem. Phys.* **1986**, *85*, 1583.
(39) Reimers, J. R.; Watts, R. O. *Chem. Phys.* **1984**, *85*, 83.
(40) Hinchliffe, A.; Bounds, D. G.; Klein, M. D.; McDonald, I. R.; Righini, R. *J. Chem. Phys.* **1981**, *74*, 1211.
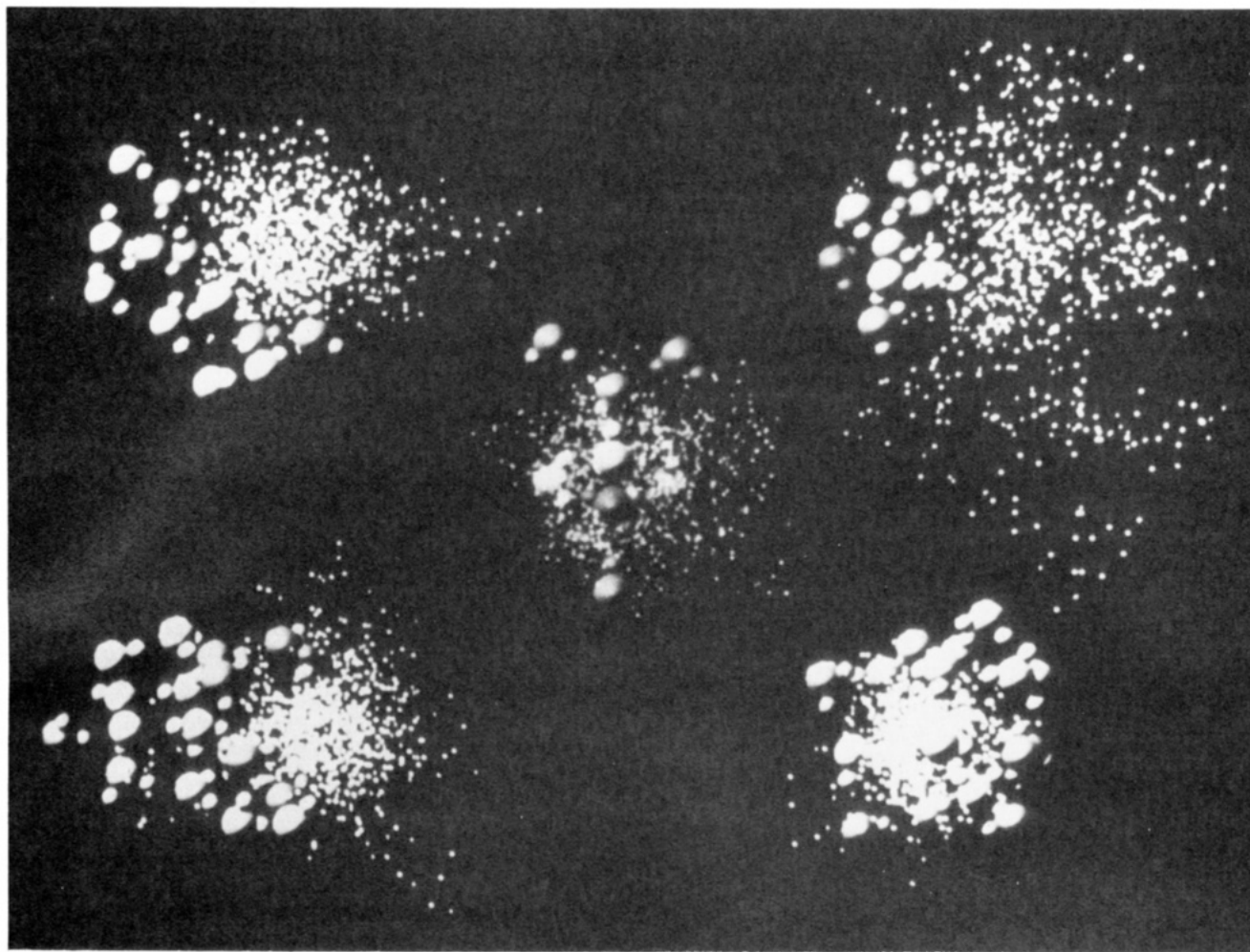
Figure 5. Cluster configurations of $(H_2O)_n^-$, from QUPID simulations.[20] Balls, large and small, correspond to oxygen and hydrogen, respectively. The dots represent the electron (bead) distribution. Shown at the center is $(H_2O)_8^-$, for a static molecular configuration as in ref 14. From top right and going counterclockwise: (i) diffuse surface $(H_2O)_8^-$; (ii) surface state of $(H_2O)_{12}^-$; (ii) surface state of $(H_2O)_{18}^-$, and (iv) internal state of $(H_2O)_{18}^-$. Reprinted with permission from ref 20. Copyright 1987 American Institute of Physics.

ture of medium-sized $(H_2O)_n^-$ ($n = 8$–64) clusters established the formation of an excess electron surface state. In correspondence with the alternative experimental preparation methods,[4-8] we have invoked[20,21] two initial conditions which correspond to (i) an internal and (ii) a surface state. For the smaller clusters, $n <$ 12, a surface state develops rapidly, regardless of the initial setup of the calculation. For $n = 18$ and 32 imposing an initial condition of a surface state results in a final "surface" state. Likewise, an initial internal state condition yields a final "internal" state. The electron bead distributions for these surface and internal states are portrayed in Figure 5. Figures 6 and 7 portray the size dependence of the adiabatic binding energy EABE, and the vertical binding energy EVBE, eq 9. From these energetic data we assert that there is a remarkable quantitative difference between interior and surface states of the excess electron in medium-sized water clusters. (1) Interior $(H_2O)_n^-$ clusters are energetically unstable, i.e., EABE > 0 for $n < 32$. (2) Energetic stability for surface states of $(H_2O)_n^-$ was established for $8 \leq n < 64$. (3) The values of E_c, which only weakly depend on the cluster size, are considerably lower for the surface states than for the interior states, ensuring the relative stability of the former. (4) The values of |EVBE| are considerably higher for the interior
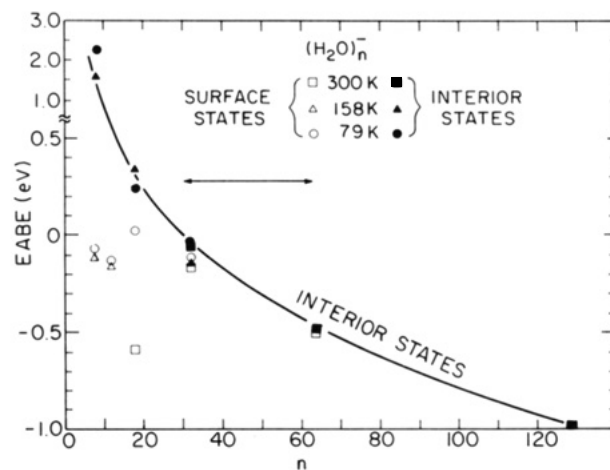

Figure 6. The size dependence of the electron adiabatic binding energy EABE in $(H_2O)_n^-$ ($n = 8$–128) clusters from QUPID simulations.[20-23] Open symbols refer to surface states while black symbols refer to interior states. The results for the interior state of the $(H_2O)_8^-$ were obtained for a static configuration of the molecules. Energetically stable surface states are exhibited for medium-sized cluster ($8 \leq n \leq 30$), and for $n = 32$ and 64 the energies of surface and interior states are about equal, while for large ($n = 128$) clusters the interior state is energetically stable. The region of crossover from surface in interior states is marked by a horizontal double arrow.
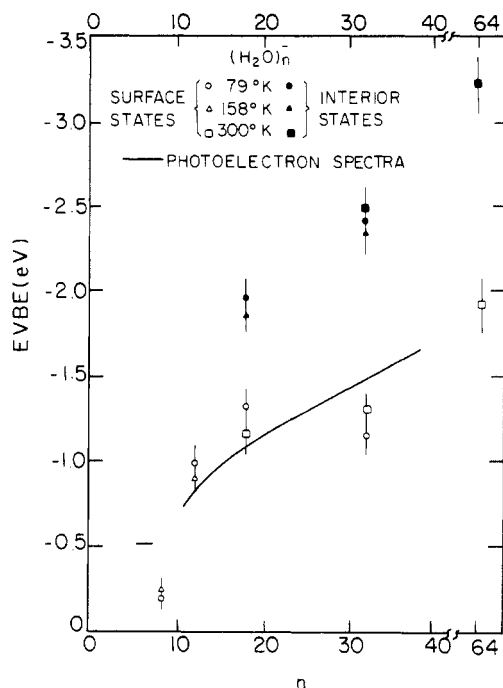
Figure 7. The size dependence of the electron vertical binding energy EVBE of $(H_2O)_n^-$ (n = 8–64) clusters. Open symbols refer to surface states while black symbols refer to interior states calculated from QUPID simulations.[20-23] The solid line represents the experimental photoelectron detachment data of K. Bowen (ref 9), for n = 11–40. The theoretical data for EVBE of surface states are in good agreement with the experimental photoelectron spectroscopy results.

states than for the surface states (Figure 6). (5) The electron localization mode in medium-sized $(H_2O)_n^-$ clusters ($8 < n < 64$) involves the formation of surface state. The surface localization mode is favored due to the dominating contribution of nearest water–electron interactions and optimization of cluster rearrangement energy. (6) The onset of electron localization in a tightly bound state in $(H_2O)_n^-$ clusters is exhibited for $n > 8$, which is in accord with experiment (n = 11).[4-8] (7) The vertical electron binding energies for the cluster–electron surface states in $(H_2O)_n^-$ (n = 8–32) are in good agreement with the experimental photoelectron spectroscopic data (Figure 7).[9]

The surface excess electron states on medium-sized $(H_2O)_n$ clusters involve a new mode of electron localization, which does not constitute the precursor of the celebrated hydrated electron.[24,36,37] We have established the ubiquity of surface electron states on clusters, which are exhibited in He_n^-,[41] some alkali–halide clusters, and medium-sized water clusters.

The Transition from Surface to Interior Electron States in Large Clusters

The size dependence of the EABEs for surface and interior states (Figure 6) implies that with increasing the size of the water cluster beyond $n \gtrsim 64$ the interior electron localization mode becomes energetically stable. The transition from surface to internal localization mode with increasing the cluster size is signified by a
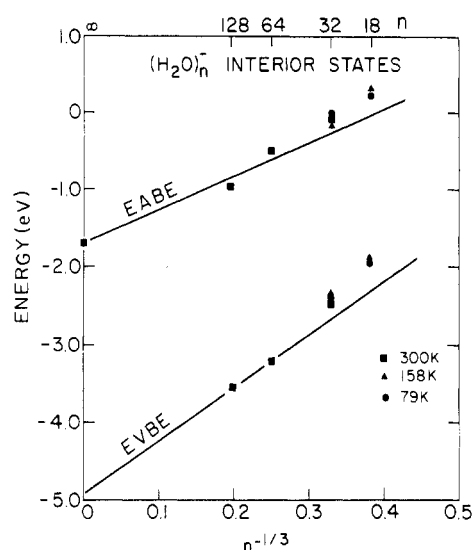
(41) Jortner, J.; Scharf, D.; Landman, U. *Excited State Spectroscopy in Solids*; Grassano, U. M., Terzi, N., Eds.; Proceedings of the International School of Physics "Enrico Fermi" July 1985; Society Italiana de Physica, Bolonga, North Holland, Amsterdam, 1987; p 438.

Figure 8. The dependence of the vertical and adiabatic binding energies of the interior excess electron state in $(H_2O)_n^-$ clusters on $n^{-1/3}$. Upper and lower sets of points represent EABE and EVBE data, respectively, at different temperatures as indicated on the figure. The black square for EABE at n = ∞ corresponds to the experimental heat of solution of an electron in water.[37] The upper straight line corresponds to $(EABE/eV) = -1.70 + 4.48n^{-1/3}$ while the lower straight line corresponds to $(EVBE/eV) = 4.90 + 6.80n^{-1/3}$. The slopes of these lines are in good agreement with the predictions of the dielectric model.

marked increase in EVBE (Figure 7), which is left as an experimental challenge.

In contrast to the case of the $(H_2O)_n^-$ cluster, we observed[23] that the onset of energetically stable electron attachment to ammonia clusters occurs exclusively via internal localization, requiring $n \gtrsim 32$ molecules, while surface states for $n < 32$ are energetically unstable. In addition, attempts to bind an electron via surface states in $n > 32$ ammonia clusters resulted in a transition to the internally localized states. The interplay between the competing effects of the interaction of the electron with the molecular constituents, the kinetic energy of localization, and the intermolecular interactions (underlying cluster reorganization) precludes the formation of stable well-bound surface states in ammonia clusters, resulting in the onset of excess electron binding via internal localization for $n \gtrsim 32$, which is in agreement with the facts of life.[4]

Bridging between Interior Excess Electron Cluster States and the Solvated Electron

The energetics of interior electron states in $(H_2O)_n^-$ and $(NH_3)_n^-$ clusters reveal a monotonic decrease of |EVBE| with increasing n. Even for the largest (n = 128 and 256) clusters studied by us, |EVBE| is considerably lower than the absolute value of the heat of solution of the electron in the bulk, indicating that there is a long wave to go from the interior electron in the cluster to the solvated electron. The interior electron localization mode in $(H_2O)_n$ and $(NH_3)_n$ clusters requires the gradual buildup of long-range attractive polarization interactions of the excess electron in large clusters. The contribution of these large polaron polarization interactions can be quantified by the application of the theory of dielectric medium effects[36] to a finite cluster.[22]

The energies of the internal excess electron states in both water and ammonia clusters exhibit a linear de-

pendence versus $n^{-1/3}$ (Figure 8). Describing the molecular cluster by a dielectric sphere of radius $\bar{R} = r_s n^{-1/3}$, where r_s is the (mean) radius of the molecular constituent, yields[22] $EABE(\bar{R}) = EVBE(\infty) + An^{-1/3}$ and $EVBE(\bar{R}) = EABE(\infty) + Bn^{-1/3}$, where $A = (e^2/2r_s)(1 - D_s^{-1})$ and $B = (e^2/2r_s)(1 + D_{op}^{-1} - 2D_s^{-1})$ where D_s and D_{op} are the static and optical dielectric constants of the material, respectively. The values of the predicted slopes A and B from the dielectric model agree with those obtained from the simulations results (Figure 8). Furthermore, an extrapolation of the EABE to $n \rightarrow \infty$

yields values in agreement with current experimental estimates, i.e., –1.7 eV for water (Figure 7) and –1.1 eV for ammonia for the bulk heats of solution of an electron in these materials.[37] Size dependence of EABE and EVBE for internal states established a continuous transition between microscopic solvation effects in finite systems and in the macroscopic polar fluids.

Conformational Analysis of Six-Membered, Sulfur-Containing Saturated Heterocycles

EUSEBIO JUARISTI

Departamento de Química, Centro de Investigación y de Estudios Avanzados del IPN, Apdo. Postal 14-740, 07000 México, D.F., México
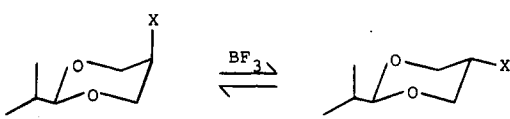
The area of organosulfur chemistry has grown rapidly during the last 20 years,[1,2] partly because the structural characteristics of sulfur have led to numerous studies of sulfur bonding, and partly because the unusual reactivity of organic sulfur compounds has resulted in the development of many useful synthetic reagents such as sulfur-stabilized carbanions and sulfur ylides. It is the purpose of this Account to show that the conformational behavior of the title systems is not only interesting but also, in some of its aspects, unusual since it reveals several conformational effects not readily explained in the light of the classical steric and dipolar interactions.

Eclipsed Conformation in *cis*-2-*tert*-Butyl-5-(*tert*-butylsulfonyl)-1,3-dioxane[3]

In a series of publications,[4,5] it was reported that repulsive interactions beyond those accounted for by steric and polar factors are responsible for the large predominance of equatorial 5-methoxy- and 5-(methylthio)-1,3-dithianes. The existence of the "repulsive gauche effect" is most likely due to the destabilizing overlap between electron lone pairs on the gauche-oriented heteroatoms, which leads to the formation of filled bonding and antibonding orbitals. In connection with this work, chemical equilibration of 5-(*tert*-butylthio)-2-isopropyl-1,3-dioxane (*cis*-1 ⇌ *trans*-1), 5-(*tert*-butylsulfinyl)-2-isopropyl-1,3-dioxane (*cis*-2 ⇌ *trans*-2), and 5-(*tert*-butylsulfonyl)-2-isopropyl-1,3-di-

Table I
Conformational Equilibria in 5-Substituted 1,3-Dioxanes 1–12

compd	X	$\Delta G°,$[a] kcal/mol	solvent	temp, °C
1	S-*t*-Bu[b]	–1.90	CHCl$_3$	23.0
2	S(O)-*t*-Bu[b]	+0.10	CHCl$_3$	23.0
3	SO$_2$-*t*-Bu[b]	–1.14	CHCl$_3$	23.0
4	SMe[c]	–1.73	ether	26.5
5	S(O)Me[c]	+0.82	CHCl$_3$	54.0
6	SO$_2$Me[c]	+1.19	CHCl$_3$	50.0
7	SC$_6$H$_5$[d]	–1.93	CHCl$_3$	25.0
8	S(O)C$_6$H$_5$[d]	+1.59	CHCl$_3$	25.0
9	SO$_2$C$_6$H$_5$[d]	–0.44	CHCl$_3$	25.0
10	S-c-C$_6$H$_{11}$[d]	e	–	–
11	S(O)-c-C$_6$H$_{11}$[d]	+0.81	CHCl$_3$	25.0
12	SO$_2$-c-C$_6$H$_{11}$[d]	0.0	CHCl$_3$	25.0

[a] Positive $\Delta G°$ values indicate axial preference. [b] Reference 3. [c] Reference 6. [d] Reference 7. [e] Unreliable measurement due to extensive decomposition.

oxane (*cis*-3 ⇌ *trans*-3) was carried out,[3] and the results were examined in light of those obtained earlier for the

Eusebio Juaristi was born in Querétaro, México, in 1950. He received the B.Sc. degree in 1972 from the Instituto Tecnológico de Monterrey (with Prof. X. A. Domínguez) and the Ph.D. degree from the University of North Carolina at Chapel Hill (with Prof. E. L. Eliel). He spent 1977–1978 as a postdoctoral fellow (with Prof. A. Streitwieser, Jr.) at the University of California, Berkeley, was appointed Associate Professor at Instituto Politécnico Nacional in 1979, and was promoted to Professor of Chemistry in 1984. In 1988, he received the Award of the Academy of Sciences of Mexico for young scientists.

(1) See, for example: Oae, S. *Organic Chemistry of Sulfur*; Plenum Press: New York, 1977. Block, E. *Reactions of Organosulfur Compounds*; Academic Press: New York, 1978. *Organic Sulfur Chemistry*; Bernardi, F., Csizmadia, I. G., Mangini, A., Ed.; Elsevier: Amsterdam, 1985.
(2) For an earlier Account, see: Eliel, E. L. *Acc. Chem. Res.* 1970, 3, 1–8.
(3) Juaristi, E.; Martínez, R.; Méndez, R.; Toscano, R. A.; Soriano-Garcia, M.; Eliel, E. L.; Petsom, A.; Glass, R. S. *J. Org. Chem.* 1987, 52, 3806–3811.
(4) Zefirov, N. S.; Blagoveshchensky, V. S.; Kazimirchik, I. V.; Surova, N. S. *Tetrahedron* 1971, 27, 3111–3118. Zefirov, N. S.; Gurvich, L. G.; Shashkov, A. S.; Krimer, M. Z.; Vorob'eva, E. A. *Tetrahedron* 1976, 32, 1211–1219.